CXCR4 promotes B cell egress from Peyer's patches

Timothy H. Schmidt, Oliver Bannard, Elizabeth E. Gray, and Jason G. Cyster

Howard Hughes Medical Institute and Department of Microbiology & Immunology, University of California, San Francisco, San Francisco, CA 94143

Peyer's patches (PPs) play a central role in supporting B cell responses against intestinal antigens, yet the factors controlling B cell passage through these mucosal lymphoid tissues are incompletely understood. We report that, in mixed chimeras, CXCR4-deficient B cells accumulate in PPs compared with their representation in other lymphoid tissues. CXCR4-deficient B cells egress from PPs more slowly than wild-type cells, whereas CXCR5-deficient cells egress more rapidly. The CXCR4 ligand, CXCL12, is expressed by cells adjacent to lymphatic endothelial cells in a zone that abuts but minimally overlaps with the CXCL13$^+$ follicle. CXCR4-deficient B cells show reduced localization to these CXCL12$^+$ perilymphatic zones, whereas CXCR5-deficient B cells preferentially localize in these regions. By photoconverting KikGR-expressing cells within surgically exposed PPs, we provide evidence that naive B cells transit PPs with an approximate residency half-life of 10 h. When CXCR4 is lacking, KikGR$^+$ B cells show a delay in PP egress. In summary, we identify a CXCL12^{hi} perilymphatic zone in PPs that plays a role in overcoming CXCL13-mediated retention to promote B cell egress from these gut-associated lymphoid tissues.

CORRESPONDENCE
Jason G. Cyster:
jason.cyster@ucsf.edu

Abbreviations used: HEL, hen egg lysozyme; HEV, high endothelial venule; LYVE-1, lymphatic vessel endothelial hyaluronan receptor-1; MLN, mesenteric LN; PLN, peripheral LN; PP, Peyer's patch; S1PR1, sphingosine-1–phosphate receptor-1.

Humans have >100 Peyer's patches (PPs; Cornes, 1965) and there are typically 6–12 in mice (Sobhon, 1971; Azzali, 2003). These mucosal lymphoid tissues play an important role in supporting B cell responses against gut antigens, both commensal and pathogen derived (Macpherson et al., 2005). Consistent with their role in fostering B cell responses, PPs have a higher frequency of B cells (~80%) than do LNs (~30%). B cell entry to both PPs and mucosal LNs requires α4β7 integrin and mucosal addressin cell adhesion molecule-1 (Berlin et al., 1993; Bargatze et al., 1995), but PPs uniquely demonstrate a substantial CXCR5-CXCL13 contribution to the adhesion triggering step (Warnock et al., 2000; Okada et al., 2002). So far, the requirements for lymphocyte egress from PPs have appeared similar to LNs, including a strong dependence on sphingosine-1–phosphate receptor-1 (S1PR1) and on lymphatic endothelial cell–produced S1P (Pham et al., 2010). However, the anatomy of PPs is quite distinct from LNs; in LNs, lymphatic vessel endothelial hyaluronan receptor-1 (LYVE-1) expressing cortical sinuses extend into the interface of B cell follicles and T cell zones and contribute to lymphocyte exit (Grigorova et al., 2009; Sinha et al., 2009; Pham et al., 2010). In PPs, lymphatic sinuses have been described near the serosal surface and in interfollicular regions (Ohtani and Murakami, 1990; Azzali and Arcari, 2000; Gohda et al., 2008) but whether these are the main sites of lymphocyte egress has not been determined. The chemokine receptor CXCR4 is abundant on naive lymphocytes and it can promote cell entry to LNs though this function is largely redundant with that of the dominant entry receptor, CCR7 (Okada et al., 2002). In vitro, naive B cells migrate robustly to even low doses of CXCL12 (Bleul et al., 1996; Nie et al., 2004). Yet, in contrast to the prominent roles of this chemokine–receptor system in developing B cells, germinal center B cells, and plasma cells (Nagasawa et al., 1996; Hargreaves et al., 2001; Nie et al., 2004; Allen et al., 2004; Pereira et al., 2009), CXCR4 and CXCL12 have no well defined function in guiding naive B cell movements within lymphoid tissues. Mice lacking CXCR4 in all B cells were reported to have

T.H. Schmidt and O. Bannard contributed equally to this paper.
E.E. Gray's present address is Dept. of Immunology, University of Washington, Seattle, WA 98195.

The Rockefeller University Press $30.00
J. Exp. Med. 2013 Vol. 210 No. 6 1099-1107
www.jem.org/cgi/doi/10.1084/jem.20122574

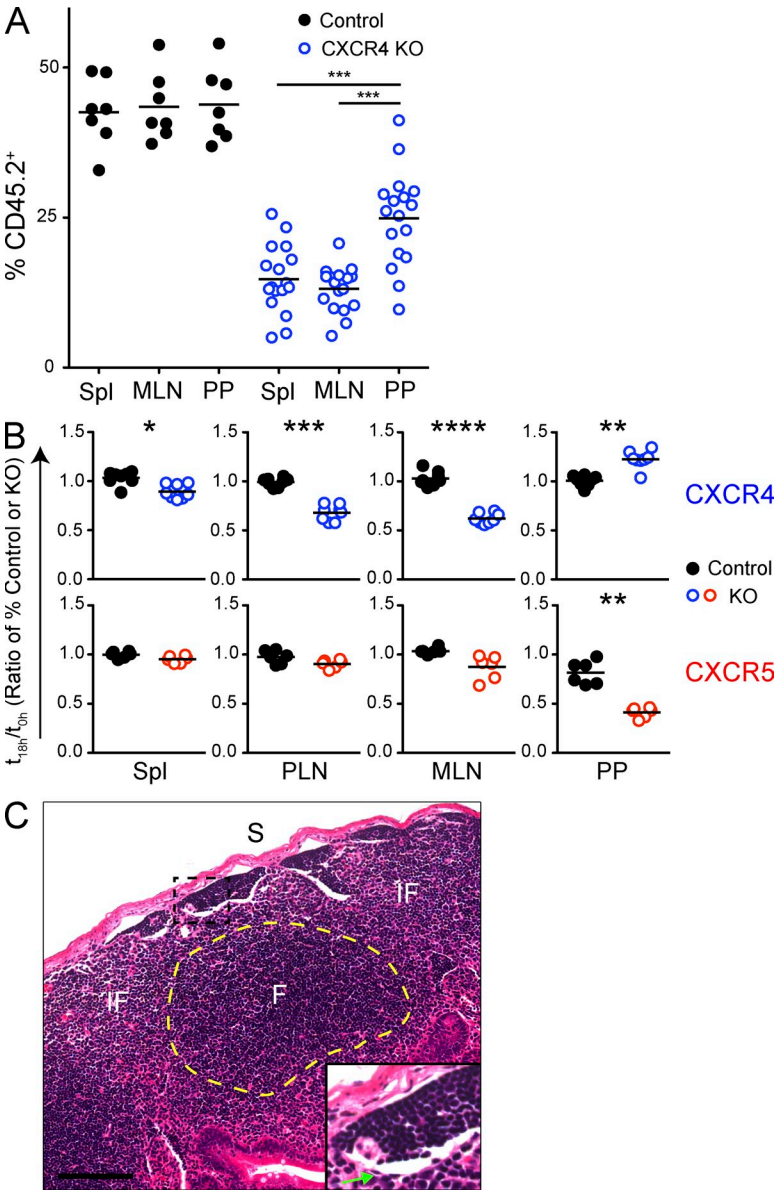

Figure 1. CXCR4 promotes and CXCR5 inhibits B cell transit through PPs. (A) Flow cytometric analysis of naive B cell distributions in CXCR4 mixed BM chimeras. Percentages of congenically marked (CD45.2+) CXCR4+/+Mb1-Cre+ (control, black, filled circles) or CXCR4fl/− Mb1-Cre+ (KO, blue, open circles) versus WT (CD45.1+) naive B cells (B220+IgDhiCD95−) in lymphoid organs. Spl, spleen. The graph represents 7 control and 17 KO mixed BM chimeric mice. (B) Flow cytometric analysis of the distribution of cotransferred control or KO versus WT naive B cells after entry blockade. Ratios of the percentages of control (solid circles) or KO (open circles) B cells among total transferred B cells 18 h after blockade of entry with α4 and αL integrin neutralizing antibodies (t_{18h}) versus immediately before entry blockade (t_{0h}) are plotted. The CXCR4 (blue, top) and CXCR5 (red, bottom) data consist of four and three experiments, respectively, with each point for a given organ representing a t_{18h}/t_{0h} pair of mice (eight and six pairs for each group, respectively). *, $P < 0.05$; **, $P < 0.01$; ***, $P < 0.001$; ****, $P < 0.0001$. P-values were obtained with Student's unpaired *t* tests comparing the mean ratios of independent experiments. (C) H&E staining of a representative fixed and paraffinized PP. The inset shows a magnified view of a subserosal lymphatic with its endothelium indicated by a green arrow. Empty space near the lymphatic is likely an artifact of sectioning. The follicle (F, dashed outline) was identified by its high density of nuclear staining. IF regions were approximated as flanking the follicle. S, serosal surface. Bar, 100 µm.

aberrant PP follicle morphology, but the basis for or significance of this effect was unknown (Nie et al., 2004).

Here we report a unique role for CXCR4 in mediating B cell access to PP lymphatic sinuses and in promoting egress from PPs into lymph. CXCR5 plays an opposing role, limiting B cell access to these sinuses and promoting B cell retention in PPs. Using a mouse transgenic for a photoconvertible protein, we confirm the PP egress–promoting role of CXCR4 and provide evidence that B cells have an ∼10 h residency time in PPs before traveling to mesenteric LNs (MLNs) and then returning to circulation.

RESULTS AND DISCUSSION

To test the possible role of CXCR4 in B lymphocyte recirculation through lymphoid organs, we generated CXCR4f/− Mb1-Cre+ (CXCR4 KO) CD45.2+:WT CD45.1+ mixed BM chimeras and examined B cell distribution in lymphoid tissues. Compared with their frequencies in spleen and MLNs, PPs showed a marked accumulation of KO over WT naive B cells (Fig. 1 A). This accumulation was not seen in control CXCR4+/+Mb1-Cre+ CD45.2+:WT CD45.1+ mixed BM chimeras (Fig. 1 A). The lower frequency of CD45.2+ B cells in spleen and MLNs of CXCR4 KO mixed BM chimeras than in the control mixed BM chimeras is a consequence of the reduced B lymphopoiesis supported by CXCR4 KO hematopoietic cells (Zou et al., 1998; Nie et al., 2004; Sugiyama et al., 2006).

To explore whether the accumulation of CXCR4-deficient cells in PPs may be a consequence of reduced egress, we performed short-term transfer experiments. CXCR4 KO and WT cells were cotransferred into WT hosts and, after a 2 d equilibration, further lymphocyte entry to PPs was blocked

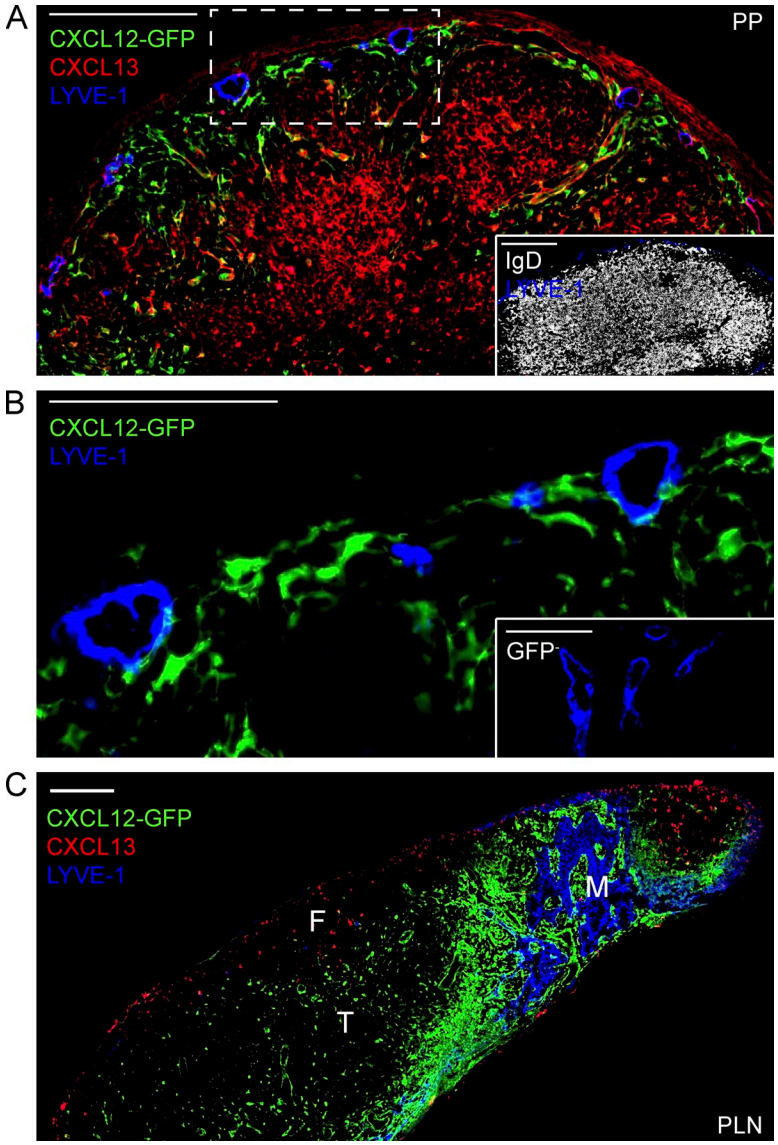

Figure 2. CXCL12 and CXCL13 are disparately distributed relative to lymphatics in PPs. Immunofluorescent detection of CXCL12 expression in GFP reporter mice in frozen sections. (A) PP follicle, oriented with its serosa on top, stained to detect GFP (reporter of CXCL12 expression, green), CXCL13 (red), and LYVE-1 (blue). The inset shows a serial section stained for IgD (white) and LYVE-1 (blue). Bars, 200 µm. (B) Magnified view of the subserosal lymphatics in A. The inset shows a similar area from a GFP^- mouse, also stained for GFP and LYVE-1. Bars, 100 µm. (C) PLN stained equivalently as the PP in A. F, follicle; T, T cell zone; M, medullary cords. Bar, 200 µm. Images are representative of more than eight PPs or PLNs.

by treatment with a combination of α4 and αL integrin neutralizing antibodies for 18 h (Lo et al., 2003). Compared with their frequency before entry blockade, CXCR4 KO cells became overrepresented selectively in PPs (Fig. 1 B). In contrast, they became underrepresented in LNs (Fig. 1 B). Similar cotransfer experiments were performed using mixtures of CXCR5 KO and WT B cells to test for a possible role of the CXCR5-CXCL13 chemokine receptor-chemokine pair in B cell transit through lymphoid organs. Based on the previous finding that CCR7-CCL21 promotes T cell retention in LNs (Pham et al., 2008), we had anticipated that CXCR5 may have a similar retention-promoting role for B cells. However, CXCR5 deficiency did not produce a statistically significant effect on the rate of B cell transit through LNs (Fig. 1 B). In contrast, there was a significantly greater reduction in CXCR5 KO than WT B cells in PPs after 18 h of entry blockade, revealing a retention-promoting role for this chemokine receptor in PPs (Fig. 1 B). These data suggested unique roles for CXCR4 and CXCR5 in promoting PP B cell egress and retention, respectively.

Lymphatic sinuses are present in both subserosal and interfollicular regions of PPs (Ohtani and Murakami, 1990; Azzali and Arcari, 2000; Gohda et al., 2008) and hematoxylin and eosin (H&E) staining of fixed and paraffin-embedded PP tissue showed that these sinuses were often filled with lymphocytes (Fig. 1 C). We next examined the distribution of CXCL12-producing cells in PPs in relation to the lymphatic sinuses, using anti–LYVE-1 to identify lymphatic endothelial cells. $LYVE\text{-}1^+$ sinuses were routinely detectable in T cell–rich interfollicular regions and in many sections large sinuses were found coursing beneath the serosal lining (Fig. 2, A and B). The distribution of CXCL12-producing cells was determined by staining for GFP in CXCL12-GFP reporter mice (Ara et al., 2003). $CXCL12\text{-}GFP^+$ cells were abundant in interfollicular and subserosal regions, including cells in close association with $LYVE\text{-}1^+$ sinuses (Fig. 2 B). Notably, the $CXCL12\text{-}GFP^+$ areas

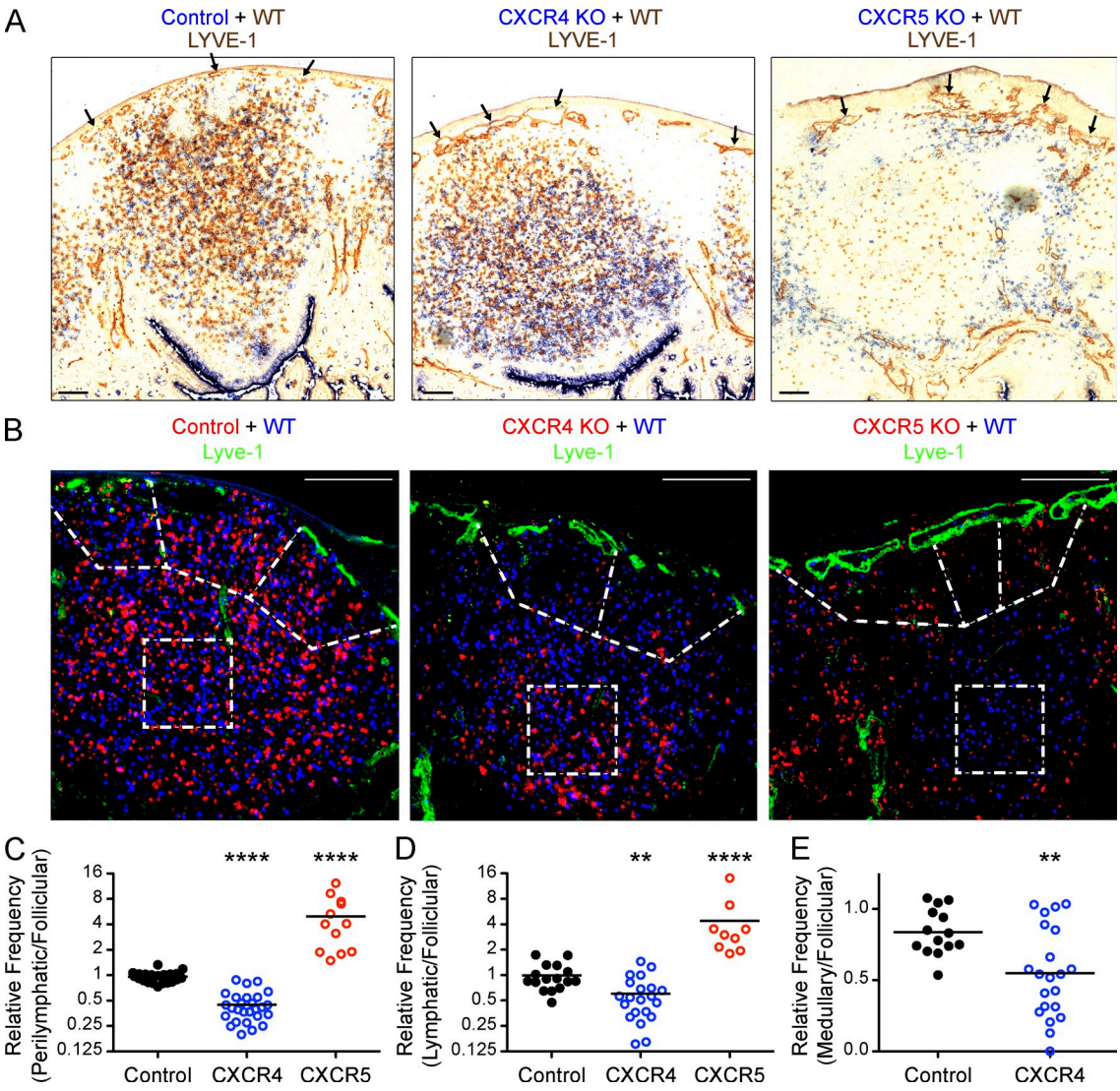

Figure 3. CXCR4 promotes and CXCR5 inhibits B cell access to PP lymphatics. (A) Immunohistochemical staining of frozen sections of PP follicles from mice that had received CXCR4$^{+/+}$Mb1-Cre^{+} control (left), CXCR4$^{fl/-}$Mb1-Cre^{+} (KO; middle), or CXCR5 KO (right) Igh^{b} splenocyte, cotransferred with splenocytes WT Ig^{HEL}-transgenic (Igh^{a}). Slides were stained with anti-IgD^{b+}IgM^{b} to detect Igh^{b+} cells (blue) and with HEL to detect Ig^{HEL} B cells (brown). Lymphatics were detected with anti–LYVE-1 (also in brown). Endogenous phosphatase activity in the epithelium is responsible for its blue staining. The PPs were oriented with their serosae on top. Arrows indicate some of the subserosal lymphatics. Similar observations were made in PPs from CXCR4 KO:WT and CXCR5 KO:WT mixed BM chimeras (three mice per condition, not depicted). Bars, 100 µm. Black arrows indicate some of the subserosal lymphatics. (B) Definition of follicular and perilymphatic areas in immunofluorescent micrographs of PPs from mice that had received mixed splenocyte transfers as in A. The 200 × 200 µm squares define the centers of the follicles. Perilymphatic areas were defined by 200 µm vectors extending from subserosal lymphatics toward the center of the follicle. Bars, 200 µm. (C) Quantification of the cell densities in the zones defined in B. Plotted are the frequencies of the indicated cell type in the perilymphatic zones relative to the center of the follicle. (D) Quantification of the frequencies of transferred cells found within or overlapping with the LYVE-1^{+} endothelia in immunofluorescent micrographs like those in B. (E) PLN quantification of the frequencies of transferred cells in 200 × 200 µm areas in the medullary cords relative to the same area in the centers of follicles in mice that had received mixed splenocyte transfers, as in B. Micrographs represent more than 10 PPs from three mice examined in three experiments per condition for both the immunohistochemical and immunofluorescence studies. Horizontal bars in C–E indicate means. **, $P < 0.01$; ****, $P < 0.0001$. P-values were obtained with Mann Whitney *t* tests.

were adjacent to but largely not overlapping with the follicular CXCL13 protein distribution, and CXCL12-GFP^{+} cells were often closely juxtaposed to LYVE-1^{+} endothelial cells (Fig. 2 A). Additionally, the CXCL13-CXCL12 transitional, often perilymphatic, margins of the follicles appeared to have lower densities of naive, IgD^{+} B cells than the centers of the follicles (Fig. 2 A, Fig. 3 A, and not depicted). Analysis of peripheral LNs (PLNs) from CXCL12-GFP reporter mice showed the expected (Hargreaves et al., 2001) high CXCL12 expression in medullary cords and lower expression throughout the T zone (Fig. 2 C). In PPs, the closely juxtaposed yet separate distributions of CXCL12 and CXCL13, along with

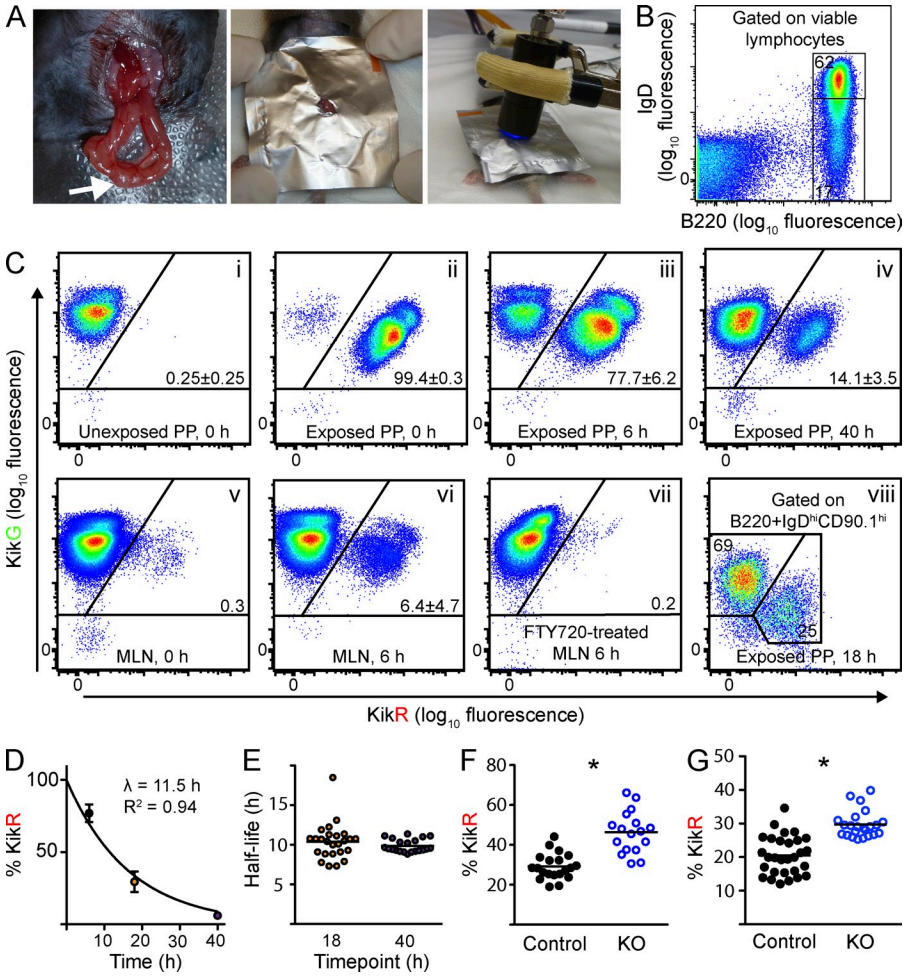

Figure 4. Kinetics of lymphocyte egress from PPs analyzed using photoconversion of KikGR-transgenic PPs and effect of B cell CXCR4 deficiency. (A) PP violet light exposure procedure. (Left) Mouse abdomen showing incision and exteriorized segment of small intestine. The arrow indicates a PP. (Middle) Sterile foil is placed over the surgical site to isolate the PP. (Right) PP is exposed to violet light from a 415 nm LED source for 3 min before replacement into the peritoneal cavity. (B) Representative flow cytometry plot showing gating for naive, B220^{+}IgD^{hi} B cells. (C) FACS plots of naive B cells in PPs (i–iv and viii) and MLNs (v–vii) from KikGR transgenic (i–vii) or transduced (viii) mice. KikG (unconverted) and KikR (converted) profiles at 0 h (i, ii, and v), 6 h (iii, vi, and vii), 18 h (viii) and 40 h (iv) after surgery. 0 h plots represent 12 and 8 PPs for unconverted and converted, respectively, and 2 MLNs, from two mice. MLN at 6 h represents five mice. The 40 h plot represents three mice. (vii) MLN from mouse treated with FTY720 for 16 h before PP photoconversion. (viii) PP from a chimera reconstituted with KikGR-transduced BM. Lower KikGR expression in the transduced cells results in diminished signal as compared with that of the transgenic mice. (D) Converted naive B cell PP retention. PPs from KikGR transgenic mice were photoconverted, after which the mice were rested for 6, 18, and 40 h. Mean (±SD), recirculation-corrected percentages (see Methods) of converted, KikR naive B cells remaining in individual, exposed PPs are fit to a single-order exponential decay curve. 6 h represents 27 PP from five mice; 18 h, 25 PP from five mice; 40 h, 21 PP from three mice. The figure represents seven independent experiments. (E) Naive B cell residency half-life values were calculated (see Materials and methods) for each exposed PP (from C) from mice rested for 18 and 40 h based on their recirculation-corrected frequencies of KikR^{+} cells. (F and G) Frequencies of KikR^{+} naive B cells remaining after 18 h in the exposed PPs of KikGR-transduced CXCR4$^{+/+}$Mb1-Cre^{+} (Control) and CXCR4$^{fl/-}$Mb1-Cre^{+} (KO) BM chimeras (F) and WT mice transferred with splenocytes from those BM chimeras (G). The graphs represent three and four pairs of mice from three and four experiments, respectively. Horizontal bars in E–G indicate means. *, $P < 0.05$. P-values were obtained with Student's unpaired *t* tests of the mean percentage of KikR values obtained from each experiment.

their potentially opposing roles in dictating B cell transit time, suggested that CXCR4 and CXCR5 might dictate access to lymphatic sinuses in these mucosal structures.

To determine how CXCL12-CXCR4 influenced B cell positioning in PPs, we immunohistochemically examined the distribution of transferred KO (Igh^{b+}) and WT (hen egg lysozyme [HEL]–binding, B cell receptor transgenic) B cells in WT, Igh^{a+} hosts. In control experiments, the Igh^{b+} and HEL^{+} B cells were codistributed in follicles and perilymphatic areas (Fig. 3 A), establishing that the Ig^{HEL} transgene did not alter B cell distribution in PPs. In contrast, in CXCR4 KO:WT cotransfers, the KO B cells were localized within follicles and were markedly underrepresented in perilymphatic regions (Fig. 3 A). Reciprocally, CXCR5 KO B cells were excluded from PP follicles, as expected (Förster et al., 1996), and were enriched in areas adjacent to lymphatic vessels (Fig. 3 A). Similar observations were made when sections were examined by three-color immunofluorescence microscopy to better distinguish LYVE-1^{+} lymphatics and transferred cells (Fig. 3 B). Enumeration of cells within 200 μm of subserosal lymphatics established that CXCR4 KO cells were significantly underrepresented in these areas, whereas CXCR5 KO cells were overrepresented, compared with their frequencies in the center of the follicle (Fig. 3 C). Similarly, enumeration of cells overlapping with or internal to the LYVE-1^{+} lymphatic endothelial staining showed a paucity of CXCR4 KO cells and an enrichment of CXCR5 KO cells (Fig. 3 D). These observations are consistent with a role for CXCR4 in promoting B cell access to PP egress sites and for CXCR5 in antagonizing such access. In PLNs, cell distributions were more variable but CXCR4 KO cells were, on average, underrepresented in medullary regions (Fig. 3 E). Despite advances in our knowledge of lymphocyte egress from LNs, the contribution of medullary regions to this process has been difficult to define as a result of their complex

Table 1. The percentages, ±SD, of KikR$^+$ lymphocytes in lymphoid organs and blood of KikGR-transgenic mice, 18 h after surgery to photoconvert their accessible PPs

Tissue	Retention or arrival	Naive B	Naive CD4	Naive CD8	Effector CD4	Effector CD8
PP	Retention	30.1 ± 5.9	7.4 ± 2.5	5.2 ± 1.7	85.1 ± 7.4	58.6 ± 16.0
MLN	Arrival	10.0 ± 4.2	3.8 ± 1.0	3.5 ± 1.0	2.7 ± 0.5	2.3 ± 0.5
PLN	Arrival	1.7 ± 0.5	1.9 ± 0.3	1.4 ± 0.3	0.2 ± 0.2	0.3 ± 0.3
Spleen	Arrival	3.5 ± 0.6	2.3 ± 0.4	1.6 ± 0.3	1.9 ± 0.5	0.4 ± 0.1
Blood	Arrival	7.4 ± 0.6	2.3 ± 0.4	1.4 ± 0.3	0.5 ± 0.1	0.4 ± 0.1

Naive B cells were defined as B220$^+$IgD$^+$. Photoconverted germinal center B cells (defined as B220$^+$IgD^{lo}CD95$^+$ or B220$^+$IgD^{lo}CD95$^+$GL7$^+$) in PPs decreased in KikR over 18 h but remained at high frequency (91.2 ± 2.5%). Naive T cells were defined as CD44$^-$CD62L$^+$ and effector T cells as CD44$^+$CD62L$^-$. The data represent five mice.

anatomy and high content of LYVE-1$^+$ macrophages (Wei et al., 2005; Grigorova et al., 2009, 2010; Sinha et al., 2009).

As an independent approach to measure lymphocyte egress rates from PPs, we adapted the photoconversion procedure of time stamping cells expressing a photoconvertible protein, Kaede, in LNs (Tomura et al., 2008, 2010) and skin (Tomura et al., 2010) to PPs. We used transgenic mice ubiquitously expressing the green-to-red, irreversibly photoconvertible protein KikGR (Tsutsui et al., 2005; Nowotschin and Hadjantonakis, 2009). PPs were surgically exposed through an ∼1.5 cm incision in the midline just below the costal margin and exposed to violet light for 3 min while protecting the surrounding tissue from light exposure using sterile foil (Fig. 4 A). The PP was then returned to the abdomen and a second PP accessed and violet light exposed. Typically, four to seven PPs were converted per mouse, leaving two to three PPs unexposed to serve as internal controls. When PPs were isolated immediately after the procedure and analyzed for naive IgD^{hi}B220$^+$ B cells (Fig. 4 B), 99.4% (SD = 0.3%, n = 8 PPs in two mice) of the cells in violet light exposed PPs had undergone the green to red conversion (Fig. 4 C, ii), whereas very few cells in the control PPs (Fig. 4 C, i) were converted (0.25 ± 0.25%, n = 12 PPs in two mice). The spleen and PLN contained a very small frequency (<0.5%) of partially converted cells at 0 h after surgery (unpublished data), which may have been cells partially photoconverted within blood vessels or early PP emigrants. When mice were examined 6 h after photoconversion, the frequency of converted naive B cells in individual PPs was reduced to 77.7% (SD = 6.2%, n = 27 PPs in five mice; Fig. 4 C, iii), whereas converted cells were now detected in circulation (not depicted) and MLNs (Fig. 4 C, vi) at rates higher than those observed immediately after PP conversion (Fig. 4 C, v). Analysis of PPs at 40 h showed that the red fluorescence intensity of converted naive B cells had decayed only slightly compared with the earlier time points, consistent with other data (Tomura et al., 2008), and showed that most of the converted cells had exited the PPs by this time (Fig. 4 C, vii). In contrast, germinal center B cells showed much greater loss of red fluorescence even after 18 h, consistent with dilution of the photoconverted protein by cell division (unpublished data).

Importantly, at both 6 and 18 h, converted cells were present at a higher frequency in MLNs than in other LNs, consistent with movement of PP cells to MLNs via the mesenteric lymphatic (Table 1). When mice were treated with FTY720 to block lymphocyte S1PR1 function (Matloubian et al., 2004) before PP photoconversion, very few photoconverted cells were found in MLNs or other lymphoid organs after 6 h (Fig. 4 C, vii; and not depicted). These data demonstrate the specificity of the photoconversion and confirm the crucial role of S1PR1 and S1P in lymphocyte egress from PPs (Pham et al., 2010). Plotting the frequencies of photoconverted naive B cells remaining in individual PPs after 6, 18, and 40 h revealed a single order decay curve with a half-life of 11.5 h (Fig. 4 C). Calculation of the apparent half-lives of naive B cells within individual PPs at the later time points—thereby allowing at least 18 h for recovery from surgical stress—revealed mean naive B cell half-lives of ∼10 h (Fig. 4 D). An assessment of all photoconverted cells remaining in PPs at 18 h showed that there was a greater exchange of naive CD4 and CD8 T cells than B cells, indicating that naive T cells exit PPs more rapidly than B cells (Table 1). Effector CD4 and CD8 T cells in PPs were replaced by newly arriving cells considerably less rapidly than naive cells (Table 1). The low rate of effector CD4 T cell egress is consistent with many of these cells being follicular helper T cells that are known to have little S1PR1 expression and to reside within B cell follicles (Rasheed et al., 2006; Crotty, 2011).

Having established a KikGR photoconversion time stamping procedure for PPs, we next applied this approach to test the egress-promoting role of CXCR4 in naive B cells. PP cells in KikGR transduced CXCR4$^{f/-}$Mb1-Cre$^+$ and CXCR4$^{+/+}$ Mb1-Cre$^+$ BM chimeras were time stamped and analyzed 18 h later, gating on cells expressing the CD90.1 (Thy1.1) reporter and then determining the frequency of photoconverted (red) cells remaining in the PP (Fig. 4 C, viii). Summarizing data from several animals revealed that a greater fraction of CXCR4-deficient than control B cells remained converted in PPs at 18 h, indicating a slower egress rate (Fig. 4 F). To control for possible indirect effects on PP organization of CXCR4 deficiency in all B cells, we performed similar time stamping experiments in WT mice that had received transfers of cells from KikGR transduced CXCR4$^{f/-}$Mb1-Cre$^+$ and CXCR4$^{+/+}$Mb1-Cre$^+$ BM chimeras. Again, when the frequency of red cells remaining in photoconverted PPs was analyzed after 18 h, a significantly greater fraction of CXCR4-deficient than control B cells were retained (Fig. 4 F).

Concluding Remarks

The above findings suggest a model where, after CXCR5-CXCL13–mediated entry to PP follicles, B cell access to subserosal and interfollicular lymphatic vessels is promoted by CXCR4-CXCL12 and antagonized by CXCR5-CXCL13. It is notable that the egress-promoting role of CXCR4 appears to be restricted to PPs. This might reflect PPs' unique anatomical organization, requiring an additional factor to facilitate B cell access to lymphatic sinuses. Consistent with this notion, a recent study identified an essential role for lymphoid tissue inducer (LTi) cells in promoting organization of postnatal PPs but not LNs through sequential movement from a $CXCL13^+$ zone to an adjacent $CXCL12^+$ zone (Nakagawa et al., 2013). The ∼10 h half-life of B cell residency in PPs is shorter than the ∼16 h time reported for LNs (Tomura et al., 2008). Although we cannot exclude the possibility that differences in the surgical procedures between studies contributes to the different rates, we suggest that the egress-promoting role of CXCR4 in PPs contributes to the more rapid transit from PPs. It is also possible that differences in B cell entry pathways are involved. In PPs, B cells enter through high endothelial venules (HEVs) that often course through the follicle (Miura et al., 1995; Warnock et al., 2000; Okada et al., 2002). In contrast, HEVs in LNs are situated in extrafollicular regions (von Andrian and Mempel, 2003) and recent B cell immigrants to LNs dwell in the perivenular space near the HEVs for a few hours before migrating to the follicle (Park et al., 2012). Given the presence of CXCL12 in association with LN HEVs (Okada et al., 2002), it seems possible that this distinct organization not only contributes to the longer B cell transit time through LNs but also accounts for why CXCR4 had a slight B cell retention effect in LNs, a possibility which warrants future investigation. In addition, T cells can migrate from medullary sinuses into the medulla (Braun et al., 2011) and egressing lymphocytes have been observed to move back from lymphatic sinuses to the LN parenchyma (Sinha et al., 2009; Grigorova et al., 2009). The reduced representation of CXCR4-deficient B cells in medullary regions might indicate that B cells passing from cortical to medullary sinuses occasionally return to the tissue parenchyma in a CXCR4-dependent manner, promoting increased residence time in the LN. Finally, our findings suggest a finely tuned balance of CXCR4 and CXCR5 function in PP B cells. The opposing roles of CXCR4 and CXCR5 raise the possibility that small changes in the abundance or function of either receptor might alter the egress rate. Thus, it will be important in future work to determine whether CXCR4 or CXCR5 function changes over time (for example, as a result of desensitization by ligand exposure [Park et al., 2012]) after B cell entry into PPs. Studies on LNs have shown that S1PR1 is an important point of egress regulation (Matloubian et al., 2004; Shiow et al., 2006). It would be interesting to determine whether B cell CXCR4 serves as a point of PP egress regulation during mucosal immune responses.

MATERIALS AND METHODS

Mice and retroviral transduction. C57BL/6 (01C55, C57BL/6NCr) and $CD45.1^+$ congenic (01B96, B6-LY5.2/Cr) mice were obtained from the National Cancer Institute. These mice were used as cotransfer donors and recipients (Fig. 1). We received mice with conditional and deleted CXCR4 alleles from Y.R. Zou (The Feinstein Institute for Medical Research, Manhasset, NY) and D. Littman (New York University, New York, NY). $CXCR4^{+/fl}$ mice (Nie et al., 2004) were crossed to $CXCR4^{+/-}$ mice (Zou et al., 1998) heterozygous for *Mb1*Cre ($Cd79a^{tm1(cre)Reth}$, MGI:3687451) provided by M. Reth (Max-Planck Institute of Immunobiology, Freiburg, Germany; Hobeika et al., 2006). $CXCR5^{-/-}$ mice (Förster et al., 1996) were received from R. Forster (Hannover Medical School, Hannover, Germany) and M. Lipp (Max Delbrück Center, Berlin, Germany) and backcrossed at least 10 generations to B6. CXCL12-GFP knockin mice (Ara et al., 2003), B6 crossed to CD1 one generation, were provided by S. Pleasure's laboratory (University of California, San Francisco [UCSF]), which received the mice originally from the Nagasawa laboratory (Kyoto University, Kyoto, Japan). For the CXCR4 and CXCR5 localization transfer recipients (Fig. 3), Igh^a (The Jackson Laboratory; 001317, B6.Cg-Igha Thy1a Gpi1a/J) mice and Ig^{HEL} (MD4) transgenic mice were bred in our colony. *CAG::KikGR*$^{Tg/+}$ (013753, Tg(CAG-KikGR)33Hadj/J; Nowotschin and Hadjantonakis, 2009) mice were purchased from The Jackson Laboratory. *CAG::KikGR*$^{Tg/+}$ mice were received on an outbred ICR strain background and backcrossed to C57BL/6 for two to four generations before use. BM was transduced as previously described (Green et al., 2011) with virus produced by Platinum E cells (Cell Biolabs) transfected with the MSCV CD90.1 (Thy1.1) retroviral vector carrying CoralHueTN KikGR1 (MBL, AM-V0081). The control and CXCR4 KO transduced chimeras had 70–80% and 50–80% $B220^+$ lymphocytes in their PPs, respectively. BM chimeras were produced by lethally irradiating host mice with a split dose of 1,100–1,300 rad, followed by i.v. transfer of BM. Chimeras were analyzed at least 7 wk after irradiation. For PP egress blockade, mice were treated with 1 mg/kg FTY720 (Cayman Chemicals) in PBS for 18 h before surgery. Animals were housed in a specific pathogen–free environment in the Laboratory Animal Research Center at UCSF, and all animal protocols were approved by the UCSF Institutional Animal Care and Use Committee.

Short-term transfers and entry blockade. RBC-lysed, CD45 congenically distinct mutant or matched control and WT splenocytes were mixed and labeled with 500 nM CFSE in 1% FBS in RPMI for 8 min. Splenocytes were mixed such that control and CXCR4 KO naive B cells represented ∼50% of transferred B cells and CXCR5 KO naive B cells represented ∼50–80% of transferred B cells. >50% CXCR5 KO B cell input proportions were used in two experiments to achieve closer to 50% ratios in the PPs. CXCR5 KO B cell proportions at 0 h were relatively low in PPs as compared with other lymphoid organs because of an expected PP-specific entry defect (Okada et al., 2002). After 2 d of equilibration, lymphoid entry blockade with a combination of α4 (Bio X-Cell; clone PS/2, rat IgG2b) and αL (Bio Express; clone M17/4, rat IgG2a) integrin neutralizing antibodies for 18 h was performed as previously described (Lo et al., 2003).

Histology, immunohistochemistry, and immunofluorescence. During harvest, care was taken not to put any pressure on the PPs to preserve their lymphatic contents. To that end, the small intestine was cut into three to four sections and flushed with PBS through a 19 G needle to remove the intestinal contents. Then the PPs were excised, still attached to a ring of intestine, with scissors. For paraffinization and H&E staining, PPs were fixed in 4% PFA in PBS for 4 h at 4°C. They were then washed five times for 10 min each in PBS at 4°C. The tissues were then dehydrated stepwise, with 1 h of 30% ethanol, followed by 1 h of 20%, and then 70% overnight. For GFP fixation, PPs were fixed as above. They were then dehydrated stepwise, starting with 30 min of 10% sucrose in PBS, followed by 30 min of 20%, and finally 30% overnight. The sucrose solution was rinsed in OCT and the tissues were frozen as normal. 7 µm frozen sections were incubated with primary antibodies for 2–4 h at room temperature; secondary and tertiary antibodies were applied for 1 h. To detect Ig^{HEL} (MD4) B cells, the sections were preincubated with 100 ng/ml HEL for 20 min. The primary antibodies used and their concentrations were: 4 µg/ml goat CXCL13 (R&D Systems), 8 µg/ml rabbit GFP (Invitrogen), 20 µg/ml goat IgD (Cederlane), 3.2 µg/ml rat LYVE-1 (R&D

Systems), 5 µg/ml FITC CD3 (BD), 5 µg/ml FITC IgDb (BD), 5 µg/ml FITC IgMb (BD), 100 µg/ml biotinylated rabbit αHEL (Rockland). Otherwise, immunohistochemistry and immunofluorescence were done as previously described (Allen et al., 2004; Pham et al., 2010). Immunohistochemical slides were mounted with AquaMount (Thermo Fisher Scientific) and immunofluorescence slides were mounted with Fluoromount-G (Southern Biotech). Slides were imaged at room temperature with AxioVision version 4.8 using an Axio Observer Z1 microscope (Carl Zeiss), equipped with an AxioCam ICc3 camera, an ORCA-ER camera (Hamamatsu Photonics), an X-cite Series 120 lamp (Lumen Dynamics), and a plan apochromat 20× objective with a 0.8 NA.

Surgery, photoconversion, and flow cytometry. Survival surgeries were performed with proper anesthetic, sterile technique, and analgesia. They were approved by and in accordance with UCSF IACUC guidelines. A mouse was anesthetized with isoflurane, shaved, and antiseptically prepared with 0.02% chlorhexidine gluconate. The mouse was then draped and a ∼1.5 cm skin incision was made anteriorly at the midline, below the costal margin. The abdominal wall was next incised. The cecum was identified and gently externalized for localization of the small intestine. The cecum was replaced and the small intestine was systematically searched for PPs. Each PP was sequentially externalized (Fig. 4 A, left), with care taken not to directly manipulate the PP or damage the mesentery. For each PP, the surgical site was covered by a piece of sterile foil with a ∼4 mm hole punched in it to leave only the PP exposed (Fig. 4 A, middle).

A Silver LED 415 (Prizmatix), set to maximum intensity, with a high numerical aperture polymer optical fiber (core diameter, 1.5 mm) light guide and fiber collimator, was used as a 415 nm violet light source. Each PP was exposed for 3 min (Fig. 4 A, right) and immediately replaced into the peritoneal cavity to avoid drying. Exposures were not possible proximal to the ligament of Treitz. The abdominal cavity was closed with 4–0 absorbable suture and the skin was closed with an Autoclip (Thermo Fisher Scientific). The entire surgery took ∼35–45 min, depending on the number of PPs discovered. The count of exposed PPs was recorded for later analysis. Doses of ∼0.1 mg/kg buprenorphine in PBS, given subcutaneously over the left shoulder, were administered immediately before and after surgery, and every 4–12 h as needed thereafter. The mice were closely monitored for signs of pain. They were rested for 0, 6, 18, and 40 h from the time of wound closure. For the KikGR-transduced splenocyte transfer experiments, cell suspensions from single spleens were transferred into CD45 congenically distinguishable WT mice, which were then allowed to equilibrate for 48 h before photoconversion surgery.

Cell suspensions were stained for 20 min on ice in FACS buffer (PBS with 0.1% sodium azide, 2% FBS, and1 µM EDTA). KikG was excited by a 50 mW 488 nm laser and detected through LP 505, BP 525/50, filters. KikR was excited by a 50 mW 561 nm laser and detected through a BP 582/15 filter. To correct for recirculating, converted B cells in mice rested for 18 or 40 h, the percentages of converted cells arriving in unexposed PPs at those time points were measured. Unexposed PPs were identified by their low frequencies of $KikR^+$ effector CD4 T cells relative to the frequencies of these cells in exposed PPs (∼1–3% vs. ∼80% at 40 h). 4.8%, (SE = 0.9%) and 55.3% (SE = 6.3%) of converted naive B cells in 18 and 40 h PPs, respectively, had recirculated. Thus, a correction for recirculating $KikR^+$ cell frequency was applied by subtracting the above mean recirculating backgrounds for the given time points from the observed PP $KikR^+$ frequencies to obtain retained converted cell frequencies (Fig. 4, C and D).

Statistical analysis and half-life calculation. Least-squares regression, as well as unpaired Student's and Mann Whitney *t* tests, were performed using Prism software (GraphPad). The least-squares regression to the single-order exponential decay curve included the constraints that y(0) = 100 and that it asymptotically approaches 0. To calculate half-lives, the equation $\lambda = \left[t \times \ln(2)\right] / \left[\ln\left(100 / \%R^+\right)\right]$ was used, where t is the number of post-operative hours and $\%R^+$ is the recirculation-corrected percentage of retained naive B cells.

Thanks to Jagan Muppidi for assistance with retroviral transduction, Jinping An for mouse husbandry and screening help, and Shuang Wu for generating the KiKGR MSCV construct. Thank you to Bogdana Schmidt for photographing the photoconversion surgery. Thanks to Jennifer Bolen and the UCSF Mouse Pathology core for H&E assistance. We thank T. Nagasawa, Y.R. Zou, D. Littman, R. Forster, and M. Lipp for mice.

T.H. Schmidt is supported by the UCSF Medical Scientist Training Program (MSTP) and the Biomedical Sciences (BMS) Graduate program. O. Bannard is supported by the Sir Henry Wellcome Postdoctoral Fellowship. J.G. Cyster is an Investigator of the Howard Hughes Medical Institute. This work was supported in part by National Institutes of Health grant AI74847.

The authors are not aware of any affiliations, memberships, funding, or financial holdings that might be perceived as affecting the objectivity of this study.

Submitted: 20 November 2012
Accepted: 18 April 2013

REFERENCES

Allen, C.D.C., K.M. Ansel, C. Low, R. Lesley, H. Tamamura, N. Fujii, and J.G. Cyster. 2004. Germinal center dark and light zone organization is mediated by CXCR4 and CXCR5. *Nat. Immunol.* 5:943–952. http://dx.doi.org/10.1038/ni1100

Ara, T., K. Tokoyoda, T. Sugiyama, T. Egawa, K. Kawabata, and T. Nagasawa. 2003. Long-term hematopoietic stem cells require stromal cell-derived factor-1 for colonizing bone marrow during ontogeny. *Immunity*. 19: 257–267. http://dx.doi.org/10.1016/S1074-7613(03)00201-2

Azzali, G. 2003. Structure, lymphatic vascularization and lymphocyte migration in mucosa-associated lymphoid tissue. *Immunol. Rev.* 195:178–189. http://dx.doi.org/10.1034/j.1600-065X.2003.00072.x

Azzali, G., and M.L. Arcari. 2000. Ultrastructural and three dimensional aspects of the lymphatic vessels of the absorbing peripheral lymphatic apparatus in Peyer's patches of the rabbit. *Anat. Rec.* 258:71–79. http://dx.doi.org/10.1002/(SICI)1097-0185(20000101)258:1<71::AID-AR8>3.0.CO;2-N

Bargatze, R.F., M.A. Jutila, and E.C. Butcher. 1995. Distinct roles of L-selectin and integrins alpha 4 beta 7 and LFA-1 in lymphocyte homing to Peyer's patch-HEV in situ: the multistep model confirmed and refined. *Immunity*. 3:99–108. http://dx.doi.org/10.1016/1074-7613(95)90162-0

Berlin, C., E.L. Berg, M.J. Briskin, D.P. Andrew, P.J. Kilshaw, B. Holzmann, I.L. Weissman, A. Hamann, and E.C. Butcher. 1993. Alpha 4 beta 7 integrin mediates lymphocyte binding to the mucosal vascular addressin MAdCAM-1. *Cell*. 74:185–195. http://dx.doi.org/10.1016/0092-8674(93)90305-A

Bleul, C.C., R.C. Fuhlbrigge, J.M. Casasnovas, A. Aiuti, and T.A. Springer. 1996. A highly efficacious lymphocyte chemoattractant, stromal cell–derived factor 1 (SDF-1). *J. Exp. Med.* 184:1101–1109. http://dx.doi.org/10.1084/jem.184.3.1101

Braun, A., T. Worbs, G.L. Moschovakis, S. Halle, K. Hoffmann, J. Bölter, A. Münk, and R. Förster. 2011. Afferent lymph-derived T cells and DCs use different chemokine receptor CCR7-dependent routes for entry into the lymph node and intranodal migration. *Nat. Immunol.* 12: 879–887. http://dx.doi.org/10.1038/ni.2085

Cornes, J.S. 1965. Number, size, and distribution of Peyer's patches in the human small intestine: Part I The development of Peyer's patches. *Gut*. 6:225–229. http://dx.doi.org/10.1136/gut.6.3.225

Crotty, S. 2011. Follicular helper CD4 T cells (TFH). *Annu. Rev. Immunol.* 29: 621–663. http://dx.doi.org/10.1146/annurev-immunol-031210-101400

Förster, R., A.E. Mattis, E. Kremmer, E. Wolf, G. Brem, and M. Lipp. 1996. A putative chemokine receptor, BLR1, directs B cell migration to defined lymphoid organs and specific anatomic compartments of the spleen. *Cell*. 87:1037–1047. http://dx.doi.org/10.1016/S0092-8674(00)81798-5

Gohda, M., J. Kunisawa, F. Miura, Y. Kagiyama, Y. Kurashima, M. Higuchi, I. Ishikawa, I. Ogahara, and H. Kiyono. 2008. Sphingosine 1-phosphate regulates the egress of IgA plasmablasts from Peyer's patches for intestinal IgA responses. *J. Immunol.* 180:5335–5343.

Green, J.A., K. Suzuki, B. Cho, L.D. Willison, D. Palmer, C.D.C. Allen, T.H. Schmidt, Y. Xu, R.L. Proia, S.R. Coughlin, and J.G. Cyster. 2011. The sphingosine 1-phosphate receptor $S1P_2$ maintains the homeostasis of germinal center B cells and promotes niche confinement. *Nat. Immunol.* 12:672–680. http://dx.doi.org/10.1038/ni.2047

Grigorova, I.L., S.R. Schwab, T.G. Phan, T.H.M. Pham, T. Okada, and J.G. Cyster. 2009. Cortical sinus probing, S1P1-dependent entry and

flow-based capture of egressing T cells. *Nat. Immunol.* 10:58–65. http://dx.doi.org/10.1038/ni.1682

Grigorova, I.L., M. Panteleev, and J.G. Cyster. 2010. Lymph node cortical sinus organization and relationship to lymphocyte egress dynamics and antigen exposure. *Proc. Natl. Acad. Sci. USA.* 107:20447–20452. http://dx.doi.org/10.1073/pnas.1009968107

Hargreaves, D.C., P.L. Hyman, T.T. Lu, V.N. Ngo, A. Bidgol, G. Suzuki, Y.-R. Zou, D.R. Littman, and J.G. Cyster. 2001. A coordinated change in chemokine responsiveness guides plasma cell movements. *J. Exp. Med.* 194:45–56. http://dx.doi.org/10.1084/jem.194.1.45

Hobeika, E., S. Thiemann, B. Storch, H. Jumaa, P.J. Nielsen, R. Pelanda, and M. Reth. 2006. Testing gene function early in the B cell lineage in mb1-cre mice. *Proc. Natl. Acad. Sci. USA.* 103:13789–13794. http://dx.doi.org/10.1073/pnas.0605944103

Lo, C.G., T.T. Lu, and J.G. Cyster. 2003. Integrin-dependence of lymphocyte entry into the splenic white pulp. *J. Exp. Med.* 197:353–361. http://dx.doi.org/10.1084/jem.20021569

Macpherson, A.J., M.B. Geuking, and K.D. McCoy. 2005. Immune responses that adapt the intestinal mucosa to commensal intestinal bacteria. *Immunology.* 115:153–162. http://dx.doi.org/10.1111/j.1365-2567.2005.02159.x

Matloubian, M., C.G. Lo, G. Cinamon, M.J. Lesneski, Y. Xu, V. Brinkmann, M.L. Allende, R.L. Proia, and J.G. Cyster. 2004. Lymphocyte egress from thymus and peripheral lymphoid organs is dependent on S1P receptor 1. *Nature.* 427:355–360. http://dx.doi.org/10.1038/nature02284

Miura, S., Y. Tsuzuki, D. Fukumura, H. Serizawa, M. Suematsu, I. Kurose, H. Imaeda, H. Kimura, H. Nagata, M. Tsuchiya, et al. 1995. Intravital demonstration of sequential migration process of lymphocyte subpopulations in rat Peyer's patches. *Gastroenterology.* 109:1113–1123. http://dx.doi.org/10.1016/0016-5085(95)90569-3

Nagasawa, T., S. Hirota, K. Tachibana, N. Takakura, S. Nishikawa, Y. Kitamura, N. Yoshida, H. Kikutani, and T. Kishimoto. 1996. Defects of B-cell lymphopoiesis and bone-marrow myelopoiesis in mice lacking the CXC chemokine PBSF/SDF-1. *Nature.* 382:635–638. http://dx.doi.org/10.1038/382635a0

Nakagawa, R., A. Togawa, T. Nagasawa, and S.-I. Nishikawa. 2013. Peyer's patch inducer cells play a leading role in the formation of B and T cell zone architecture. *J. Immunol.* 190:3309–3318. http://dx.doi.org/10.4049/jimmunol.1202766

Nie, Y., J. Waite, F. Brewer, M.-J. Sunshine, D.R. Littman, and Y.-R. Zou. 2004. The role of CXCR4 in maintaining peripheral B cell compartments and humoral immunity. *J. Exp. Med.* 200:1145–1156. http://dx.doi.org/10.1084/jem.20041185

Nowotschin, S., and A.-K. Hadjantonakis. 2009. Use of KikGR a photoconvertible green-to-red fluorescent protein for cell labeling and lineage analysis in ES cells and mouse embryos. *BMC Dev. Biol.* 9:49. http://dx.doi.org/10.1186/1471-213X-9-49

Ohtani, O., and T. Murakami. 1990. Organization of the lymphatic vessels and their relationships to blood vessels in rabbit Peyer's patches. *Arch. Histol. Cytol.* 53:155–164. http://dx.doi.org/10.1679/aohc.53.Suppl_155

Okada, T., V.N. Ngo, E.H. Ekland, R. Förster, M. Lipp, D.R. Littman, and J.G. Cyster. 2002. Chemokine requirements for B cell entry to lymph nodes and Peyer's patches. *J. Exp. Med.* 196:65–75. http://dx.doi.org/10.1084/jem.20020201

Park, C., I.-Y. Hwang, R.K. Sinha, O. Kamenyeva, M.D. Davis, and J.H. Kehrl. 2012. Lymph node B lymphocyte trafficking is constrained by anatomy and highly dependent upon chemoattractant desensitization. *Blood.* 119:978–989. http://dx.doi.org/10.1182/blood-2011-06-364273

Pereira, J.P., J. An, Y. Xu, Y. Huang, and J.G. Cyster. 2009. Cannabinoid receptor 2 mediates the retention of immature B cells in bone marrow sinusoids. *Nat. Immunol.* 10:403–411. http://dx.doi.org/10.1038/ni.1710

Pham, T.H.M., T. Okada, M. Matloubian, C.G. Lo, and J.G. Cyster. 2008. S1P1 receptor signaling overrides retention mediated by G α i-coupled receptors to promote T cell egress. *Immunity.* 28:122–133. http://dx.doi.org/10.1016/j.immuni.2007.11.017

Pham, T.H.M., P. Baluk, Y. Xu, I. Grigorova, A.J. Bankovich, R. Pappu, S.R. Coughlin, D.M. McDonald, S.R. Schwab, and J.G. Cyster. 2010. Lymphatic endothelial cell sphingosine kinase activity is required for lymphocyte egress and lymphatic patterning. *J. Exp. Med.* 207:17–27. http://dx.doi.org/10.1084/jem.20091619

Rasheed, A.-U., H.-P. Rahn, F. Sallusto, M. Lipp, and G. Müller. 2006. Follicular B helper T cell activity is confined to CXCR5(hi)ICOS(hi) CD4 T cells and is independent of CD57 expression. *Eur. J. Immunol.* 36:1892–1903. http://dx.doi.org/10.1002/eji.200636136

Shiow, L.R., D.B. Rosen, N. Brdicková, Y. Xu, J. An, L.L. Lanier, J.G. Cyster, and M. Matloubian. 2006. CD69 acts downstream of interferon-α/β to inhibit S1P1 and lymphocyte egress from lymphoid organs. *Nature.* 440:540–544. http://dx.doi.org/10.1038/nature04606

Sinha, R.K., C. Park, I.-Y. Hwang, M.D. Davis, and J.H. Kehrl. 2009. B lymphocytes exit lymph nodes through cortical lymphatic sinusoids by a mechanism independent of sphingosine-1-phosphate-mediated chemotaxis. *Immunity.* 30:434–446. http://dx.doi.org/10.1016/j.immuni.2008.12.018

Sobhon, P. 1971. The light and the electron microscopic studies of Peyer's patches in non germ-free adult mice. *J. Morphol.* 135:457–481. http://dx.doi.org/10.1002/jmor.1051350404

Sugiyama, T., H. Kohara, M. Noda, and T. Nagasawa. 2006. Maintenance of the hematopoietic stem cell pool by CXCL12-CXCR4 chemokine signaling in bone marrow stromal cell niches. *Immunity.* 25:977–988. http://dx.doi.org/10.1016/j.immuni.2006.10.016

Tomura, M., N. Yoshida, J. Tanaka, S. Karasawa, Y. Miwa, A. Miyawaki, and O. Kanagawa. 2008. Monitoring cellular movement in vivo with photoconvertible fluorescence protein "Kaede" transgenic mice. *Proc. Natl. Acad. Sci. USA.* 105:10871–10876. http://dx.doi.org/10.1073/pnas.0802278105

Tomura, M., T. Honda, H. Tanizaki, A. Otsuka, G. Egawa, Y. Tokura, H. Waldmann, S. Hori, J.G. Cyster, T. Watanabe, et al. 2010. Activated regulatory T cells are the major T cell type emigrating from the skin during a cutaneous immune response in mice. *J. Clin. Invest.* 120:883–893. http://dx.doi.org/10.1172/JCI40926

Tsutsui, H., S. Karasawa, H. Shimizu, N. Nukina, and A. Miyawaki. 2005. Semi-rational engineering of a coral fluorescent protein into an efficient highlighter. *EMBO Rep.* 6:233–238. http://dx.doi.org/10.1038/sj.embor.7400361

von Andrian, U.H., and T.R. Mempel. 2003. Homing and cellular traffic in lymph nodes. *Nat. Rev. Immunol.* 3:867–878. http://dx.doi.org/10.1038/nri1222

Warnock, R.A., J.J. Campbell, M.E. Dorf, A. Matsuzawa, L.M. McEvoy, and E.C. Butcher. 2000. The role of chemokines in the microenvironmental control of T versus B cell arrest in Peyer's patch high endothelial venules. *J. Exp. Med.* 191:77–88. http://dx.doi.org/10.1084/jem.191.1.77

Wei, S.H., H. Rosen, M.P. Matheu, M.G. Sanna, S.-K. Wang, E. Jo, C.-H. Wong, I. Parker, and M.D. Cahalan. 2005. Sphingosine 1-phosphate type 1 receptor agonism inhibits transendothelial migration of medullary T cells to lymphatic sinuses. *Nat. Immunol.* 6:1228–1235. http://dx.doi.org/10.1038/ni1269

Zou, Y.R., A.H. Kottmann, M. Kuroda, I. Taniuchi, and D.R. Littman. 1998. Function of the chemokine receptor CXCR4 in haematopoiesis and in cerebellar development. *Nature.* 393:595–599. http://dx.doi.org/10.1038/31269